Open access • Journal Article • DOI:10.1061/(ASCE)GT.1943-5606.0001781

Shearing Behavior of Tire-Derived Aggregate with Large Particle Size. II: Cyclic Simple Shear — Source link

John S. McCartney, Ismaail Ghaaowd, Patrick J. Fox, Michael J. Sanders ...+2 more authors

Institutions: University of California, San Diego, Pennsylvania State University

Published on: 01 Oct 2017 - Journal of Geotechnical and Geoenvironmental Engineering (American Society of Civil Engineers (ASCE))

Topics: Shear rate, Shearing (physics) and Simple shear

Title
Shearing Behavior of Tire-Derived Aggregate with Large Particle Size. II: Cyclic Simple Shear

Journal
JOURNAL OF GEOTECHNICAL AND GEOENVIRONMENTAL ENGINEERING, 143(10)

ISSN
1090-0241

Authors
McCartney, John S
Ghaaowd, Ismaail
Fox, Patrick J
et al.

Publication Date
2017-10-01

DOI
10.1061/(ASCE)GT.1943-5606.0001781

Peer reviewed

SHEARING BEHAVIOR OF TIRE DERIVED AGGREGATE WITH LARGE PARTICLE SIZE. II: CYCLIC SIMPLE SHEAR

by John S. McCartney, Ph.D., P.E., M.ASCE[1], Ismaail Ghaaowd, M.S., S.M. ASCE[2], Patrick J. Fox, Ph.D., P.E., F.ASCE[3], Michael J. Sanders, M.S., S.M. ASCE[4], Stuart S. Thielmann, M.S.[5], and Andrew C. Sander, M.S., S.M.ASCE[6]

ABSTRACT: Although Tire-Derived Aggregate (TDA) has been used widely as lightweight fill in civil engineering applications, the properties governing its response under cyclic loading are not well understood. Reliable data on the evolution of shear modulus and damping ratio with cyclic shear strain amplitude are needed for the prediction of the seismic response of TDA fills, especially those with larger particle sizes up to 300 mm (Type B TDA). This study presents the results of cyclic simple shear tests performed on Type B TDA using a new large-scale testing device for vertical stresses ranging from 19.3 to 76.6 kPa and shear strain amplitudes ranging from 0.1% to 10%. The shear modulus of Type B TDA has a maximum value of 3,355 kPa and decreases with increasing shear strain amplitude, which is smaller in magnitude and similar in trend to natural granular soils in this vertical stress range. Continuous volumetric contraction was observed during cyclic loading for all stress levels. The damping ratio for Type B TDA showed a different behavior from granular soils, with a relatively high magnitude of 20 to 25% at the lowest shear strain amplitude (0.1%), followed by a decreasing/increasing trend with increasing amplitude. The shear modulus was found to follow a power law relationship with vertical stress, similar to granular soils, and the damping ratio was not sensitive to vertical stress level.

---

[1] Associate Professor, Dept. of Structural Eng., Univ. of California San Diego, 9500 Gilman Dr., La Jolla, CA 92093-0085; mccartney@ucsd.edu
[2] Doctoral Candidate, Dept. of Structural Eng., Univ. of California San Diego, 9500 Gilman Dr., La Jolla, CA 92093-0085; ighaaowd@eng.ucsd.edu
[3] Shaw Professor and Head, Dept. of Civil and Environmental Engineering, The Pennsylvania State University, 212 Sackett Building, University Park, Pa 16802-1408; pjfox@engr.psu.edu
[4]Structural Engineer, Dept. of Structural Eng., Univ. of California San Diego, 9500 Gilman Dr., La Jolla, CA 92093-0085; mjsander@eng.ucsd.edu
[5]Staff Geotechnical Engineer, GeoEngineers, Inc., 1101 S Fawcett Ave # 200, Tacoma, WA 98402
[6]Structural Designer, WRK Engineers, 215 W 12th St #202, Vancouver, WA 98660

INTRODUCTION

The recycling of waste tires in the form of Tire-Derived Aggregate (TDA) as a lightweight backfill is promoted throughout the U.S., and is particularly important for states that have high rates of generation, like in California where 40 million tires are discarded every year (CalRecycle 2016a). TDA with large particle sizes up to 300 mm, referred to as Type B TDA (ASTM D6270), can be used in layers with a thickness up to 3 m for applications such as highway embankments or retaining walls (Geosyntec 2008; Ahn et al. 2014; CalRecycle 2016b). Under static loading, these systems have been shown to have comparable or superior performance to similar systems constructed with natural backfill soil (Humphrey et al. 1993; Bosscher et al. 1993; Bosscher et al. 1997; Hoppe 1998; Tweedie et al. 1998; Dickson et al. 2001; Tandon et al. 2007); however, they may also experience strong shaking in seismically-active regions such as California.

The seismic performance of retaining walls constructed with TDA has been evaluated in large-scale experiments recently by Xiao et al. (2012) and Ahn and Cheng (2014), who found that TDA has a softer response than natural granular soils and advantageous seismic characteristics such as lower dynamic earth pressures and the ability to experience large residual deformations without catastrophic failure. However, these studies did not report TDA cyclic shear properties that are needed to simulate seismic performance, such as variation of shear modulus and damping ratio with cyclic strain magnitude under different stress conditions. Although there have been studies on the cyclic properties of TDA with relatively small particle sizes mixed with natural soils (Bosscher et al. 1997; Feng and Sutterer 2000; Kaneko et al. 2003; Anastasiadis et al. 2012a, 2012b; Senetakis et al. 2012a, 2012b, Nakhei et al. 2012; Mashiri et al. 2013; Ehsani et al. 2015), the cyclic properties of Type B TDA have not been evaluated due to the need for a large testing device to accommodate the large particle size. There are also other applications where TDA may experience cyclic loading, such as a cushion material to dampen vibrations from compaction (Lee and Roh 2007), a coastal liquefaction mitigation measure (Hazarika et al. 2008), and a seismic isolation layer for building foundations (Tsang 2008). Accordingly, more data and information are needed on the dynamic properties of Type B TDA for earthquake engineering design.

To address this need, Fox et al. (2017) developed a novel large-scale combination direct shear/simple shear device for Type B TDA that can accommodate specimens measuring 3048 mm × 1219 mm in plan and up to 1830 m in height. This paper presents the results of cyclic simple shear tests on Type B TDA material using this device. The data include shear modulus, damping ratio, and volumetric strain under a range of vertical stresses and cyclic shear strain amplitudes. A companion paper (Ghaaowd et al. 2017) presents corresponding data for TDA internal direct shear and TDA-concrete interface direct shear tests obtained using the same device.

BACKGROUND

Feng and Sutterer (2000) noted several characteristics of granulated rubber from waste tires that make the dynamic response potentially different from natural soils, including elastic behavior over a wider range of deformation, a relatively ductile stress-strain curve, and more extensive recovery from large deformations when stresses are removed. Further, the granulated rubber particles have a lower modulus of elasticity than soil particles, and have a Poisson's ratio of nearly 0.5 indicating low volume compressibility.

Three previous studies investigated the cyclic response of TDA, as described in Table 1. Feng and Sutterer (2000) performed resonant column tests to measure the shear modulus and damping ratio of granulated rubber (particle size = 2.00 to 4.76 mm) mixed with Ottawa sand, and found that the addition of sand produced an increase in shear modulus and reduction in damping ratio. They also tested pure granulated rubber and measured shear modulus values ranging from 1100 to 2800 kPa for effective stresses ranging from 69 to 483 kPa and shear strains ranging from 0.003 to 0.1%. This range of effective stress is much greater than expected for many TDA construction applications, such as retaining walls or embankments, and thus additional work is needed to understand variations in shear modulus at lower effective stress levels. Feng and Sutterer (2000) also observed that damping ratio of granulated rubber was not particularly sensitive to effective stress, and had an initially high value of 4.5 to 6.0%. In most of their tests, the damping ratio increased with increasing shear strain amplitude, while in one test a small decrease was observed initially followed by an increase at higher shear strain amplitudes.

Kaneko et al. (2003) performed cyclic shear strain tests on saturated specimens of TDA in the form of tire chips having a maximum particle size of 1.1 mm. The measured hysteresis loops have shapes similar to those for natural soils, with a clear peak value at the point of strain reversal. Kaneko et al. (2003) also found that, because the particles are deformable, shear strains can be accommodated with less particle sliding and rearrangement. This feature, combined with the high hydraulic conductivity, suggests that tire chips will not experience generation of excess pore water pressures during cyclic loading that may lead to liquefaction. The hysteresis loops reported by Kaneko et al. (2003) were reinterpreted by the authors to calculate shear modulus and damping ratio for different effective stress values, which are reported in Table 1. Hazarika et al. (2010) performed a cyclic simple shear tests on a saturated specimen of TDA in the form of tire chips having a maximum particle size of 1.0 mm. The hysteresis loop for this test was reinterpreted by the authors to define the shear modulus and damping ratio, which are reported in Table 1.

Several studies have investigated the shear modulus and damping ratio of soil-TDA mixtures (Feng and Sutterer 2000; Kaneko et al. 2003, Anastasiadis et al. 2012a, 2012b; Senetakis et al. 2012a, 2012b, Nakhei et al. 2012; Mashiri et al. 2013; Ehsani et al. 2015). These studies generally observed that the shear modulus decreased and the damping ratio increased with the percentage of TDA in the soil-TDA mixture. For example, Anastasiadis et al. (2012a) found that the shear modulus decreased from 45 to 10 MPa and the damping ratio increased from 0.68 to 0.40% when adding 35% TDA to soil at a confining stress of 30 kPa.

Although the resilient modulus is not as useful as the shear modulus versus cyclic shear strain relationship, studies on resilient modulus may provide further insight into the cyclic response of TDA. Bosscher et al. (1997) evaluated the resilient modulus of TDA having a maximum particle size of 75 mm, and found that the cyclic loading force-displacement hysteresis loops and resulting modulus of subgrade reaction values do not change significantly from the first cycle with continued cyclic loading. Values of resilient modulus increased from 1000 to 1900 kPa as the effective confining stress increased from 19 to 105 kPa. The subgrade reaction experimental design in the Bosscher et al. (1997) study did not allow for measurement of shear modulus and damping ratio values, or control of shear strain amplitude, and thus the results are limited in terms of TDA dynamic properties. The specimen size in these tests was also limited and could not accommodate large-size TDA material.

Two recent studies have evaluated the seismic response of TDA used as a backfill in gravity retaining walls (Ahn and Cheng 2014) and geosynthetic-reinforced retaining walls (Xiao et al. 2012). Ahn and Cheng (2014) performed a shake table test on a large-scale (2 m high) cantilever retaining structure constructed from a layer of Type B TDA and an overlying layer of sand, and found that the dynamic pressure exerted on the wall was smaller in the TDA layer. Further, the TDA experienced relatively large residual shear deformations of up to 50 mm without catastrophic failure. Xiao et al. (2012) performed a shake table test on a reduced-scale (1.6 m high) geosynthetic-reinforced retaining structure constructed from TDA with a maximum particle size of 150 mm, and compared the results with a similarly-constructed wall using only sand. The wall constructed with TDA backfill had less lateral displacement, less vertical settlement, apparent acceleration attenuation toward the top of the wall, and lower static and dynamic lateral stresses on the wall. These studies indicate that TDA backfill for retaining walls offers several advantages in comparison to natural backfill soils.

EXPERIMENTAL EQUIPMENT AND PROCEDURES

Equipment

A schematic diagram and photograph of the large-scale combination direct shear/simple shear device developed by Fox et al. (2017) are shown in Figure 1. The inside dimensions of the shearing box in simple shear mode are 3048 mm × 1219 mm in plan, with a height of 1600 mm. The specimen height used for the simple shear tests is approximately 1400 mm, which is shorter than the specimen height used in direct shear mode. The sides of the box in the direction parallel to shear consist of stacked tubular steel members, while the sides of the box in the direction perpendicular to shear consist of vertical solid steel plates. In the simple shear mode, the tubular members are pinned to the steel plates on the ends so that the box can deform as a parallelogram and induce shear strain to the TDA specimen. Two hydraulic actuators are used to provide the horizontal force and are operated in displacement-control mode. The actuator stroke allows the box to be cycled in either direction with a maximum shear strain of 30%. The horizontal displacement Δx is measured on the top of the device at a height of H = 1600 mm using a string potentiometer, which is needed to calculate the shear strain γ (=Δx/H). Transverse fins on the top and bottom surfaces of the box (i.e., above and below the specimen) are used to minimize slippage of the TDA specimen and increase the uniformity of shear stress application. Instrumentation includes a load cell for each actuator, four potentiometers (i.e., one at each corner of the box) to measure vertical displacements, a string potentiometer to measure horizontal displacements, and tiltmeters to measure vertical end plate and actuator rotations. Eight load cells were placed between the top plate and the TDA to measure uniformity of contact stress during the shearing process. The load cell measurements were nearly identical throughout shearing. Additional details regarding design and evaluation of the device are provided by Fox et al. (2017) and the companion paper (Ghaaowd et al. 2017).

Procedures

The Type B TDA material and specimen preparation procedures for the current study were the same as for the direct shear testing program described in the companion paper (Ghaaowd et al. 2017). Plastic sheeting was used to line the inside walls of the box to reduce sidewall friction, and the TDA was compacted in 100 mm-thick loose lifts using a 14.4 kN rolling and vibrating compactor and 6 passes per lift. Although the compactor weight is lower than that suggested in ASTM D6270 (90 kN), the lift thickness used in this study is smaller, and the lateral constraint provided by the box may lead to greater densities than expected in the field for the same compaction energy (Ghaaowd et al. 2017).

The testing program is summarized in Table 2 and consisted of four simple shear tests, SS1 to SS4, each conducted using a single TDA specimen to characterize the effects of vertical stress (σ = 19.3 to 76.6 kPa) and cyclic shear strain amplitude (γ_a = 0.1 to 10%) on secant shear modulus and damping ratio. Each test included multiple stages, with each stage consisting of 20 cycles of back-and-forth shearing under constant applied stress and using a triangular waveform with constant shear strain amplitude and constant actuator displacement rate of 16 mm/min. At the elevation of the string potentiometer (1600 mm), this corresponds to a displacement rate of 24 mm/min and a shear strain rate of 1.5%/min. Displacement rates for the simple shear tests are sufficiently slow that inertial forces are negligible and have no effect on the measured results. Tests SS2, SS3, and SS4 included five stages of progressively increasing shear strain amplitude (γ_a = 0.1, 0.3, 1, 3, and 10%), and test SS1 included eight stages also spanning between γ_a = 0.1% and 10%, with one reversal in between (Table 2). The tests were operated in displacement-control mode with shearing force measured at the actuators and corrected for actuator tilt from horizontal. A static waiting period of 30 minutes (i.e., γ = 0) was included between the successive stages of each test.

RESULTS

The total unit weight of TDA after compaction was approximately 5.6 kN/m^3 for each test. Dead weight loading increased the total unit weights to the initial values provided in Table 2, which range from 5.64 to 7.07 kN/m^3 and are consistent with corresponding values for the TDA direct shear tests (Ghaaowd et al. 2017). Further, this range of unit weight values is typical of TDA used in monolithic fill applications (CalRecycle 2011, 2016b). Using a specific gravity of 1.15 (Ghaaowd et al. 2017), the corresponding values of void ratio range from 1.00 to 0.60. Due to the relatively large height of TDA specimens in the current study, self-weight of the TDA material yielded an increase in vertical stress of 9.0 to 11.4 kPa from top to bottom. The variation of vertical stress across the specimen is much greater than for conventional-sized simple shear tests, in which soil self-weight is typically ignored, and may have an effect on results when material response varies nonlinearly with effective stress. Vertical stresses in Table 2 and listed in the figures are the values at specimen mid-height.

The results from test SS1 are shown in Figure 2. This was the first test performed to characterize the cyclic simple shear response of Type B TDA, and was different than the other tests. The shear strain amplitude was increased in stages up to 3%, then decreased in stages to 0.1%, after which the test was stopped. The specimen was then removed and recompacted, the vertical stress was reapplied, and shearing was started again at $\gamma_a = 3.0\%$ and then increased to 10%. The horizontal displacement time history for all stages of the test is shown in Figure 2(a). As the hydraulic actuators were operated in displacement-control mode, reversals occur regularly within each cycle and amplitude is nearly constant within each stage. The corresponding shear force values are shown in Figure 2(b). After application of a few cycles, the shear force tends to stabilize for each stage of the test. However, for some of the cycles at the highest cyclic shear strain amplitude, slack in the system due to a gap between the top loading plate and the end plates affected the force values needed to reach the target strain amplitude, as will be observed in the hysteresis loops for this test (see below). This was corrected in subsequent tests by adding spacer blocks to close this gap. Volumetric strains during cyclic shearing are shown in Figure 2(c), and indicate continuous contraction and a decreasing rate of contraction with continued cycling for each stage, similar to natural soils. After recompaction and reloading, the specimen yielded a force amplitude for $\gamma_a = 3.0\%$ that was nearly the same as the previous loading at $\gamma_a = 3.0\%$. This indicates good repeatability of cyclic shear results for the same loading conditions.

The results from tests SS2, SS3 and SS4 are shown in Figures 3, 4 and 5, respectively, and display similar behavior for higher vertical stress levels. The actuators indicate good displacement control, with the exception of one cycle during the final stage of SS2. After a few cycles, the shear force was observed to nearly stabilize during each stage of the tests. Continuous contraction was observed in all cases, and volumetric strains did not stabilize after 20 cycles for each stage similar to test SS1. This response is consistent with observations for granular soils. For example, Lee and Albaisa (1974) observed volumetric contraction for both loose and dense sands during cyclic shear loading, while Hsu and Vucetic (2004) and Whang et al. (2000) observed similar trends for compacted soils. These studies indicated that more than 100 loading cycles may be needed to reach the equilibrium state for volumetric contraction. Youd (1972) found that volumetric strain equilibrium was not reached in drained cyclic simple shear tests on sand after 10,000 cycles, although a progressively slower rate of contraction is observed with continued cycling.

A comparison of the volumetric strains after 20 cycles for each stage of the four tests is shown in Figure 6. To define the curve for test SS1, values were taken from the first loading sequence and then from the end of cyclic loading for the 3 and 10% shear strains on the reloading sequence. Similar to the findings for natural granular soils (e.g., Silver and Seed 1971; Youd 1972), vertical stress does not have a significant effect on the evolution of volumetric strain with increasing cyclic shear strain amplitude. It is also interesting that all of the tests showed volumetric contraction during cyclic shearing regardless of the applied vertical stress or initial total unit weight. This indicates that, similar to granular soils, the TDA particles continued to adjust and densify under continuous cycling, but did not ride over each other to cause dilation as occurred for the corresponding TDA monotonic direct shear tests at large displacements (Ghaaowd et al. 2017). In the direct shear tests, contraction was observed in each case until the horizontal displacement was approximately 120-150 mm, after which all specimens exhibited dilation. The amount of this initial contraction increased with the normal stress level, and the dilation response decreased with increasing normal stress.

ANALYSIS

Shear stresses were calculated by dividing measured shear force by the plan cross-sectional area of the box and shear strains were calculated by dividing applied horizontal displacement by the elevation of the displacement measurement (H = 1600 mm). The hysteresis loops for all stages of each test are shown in Figure 7. The hysteresis loops have a similar shape and are symmetric about the origin. The size of the hysteresis loops increases with increasing vertical stress, and at higher stress levels the loops for tests SS3 and SS4 are more consistent in shape than for tests SS1 and SS2. The slack in the system in test SS1 is reflected in the change in shape near the strain limits at the highest cyclic shear strain amplitude in Figure 7(a). Data from these loops were not included in the subsequent analysis of TDA secant shear modulus and damping ratio.

The backbone curves for the four tests are shown in Figure 8. Each curve was prepared by plotting the maximum shear stress against corresponding shear strain amplitude for the final (i.e., 20th) cycle of loading at each test stage. The curves display nonlinearity with increasing shear strain and are symmetric about the origin similar to the hysteresis loops. An increase in magnitude of the shear stress with increasing vertical stress is also observed, as expected. Interestingly, even at 10% shear strain, the TDA has still not reached a peak shear strength value. This is in contrast to dense sands, which would generally be expected to reach peak strength by this point (Lee and Seed 1967). Values of secant shear modulus were calculated from the peak end points of the hysteresis loops, as follows:

$$G = G_{secant} = \frac{(\tau_{max} - \tau_{min})}{(\gamma_{max} - \gamma_{min})} \tag{1}$$

Values of damping ratio indicate relative energy dissipation during cyclic shearing, and were calculated on an average basis for the 20 cycles of each testing stage as follows:

$$D = \frac{1}{4\pi}\frac{A_L}{A_T} \qquad (2)$$

where A_L is the area within the hysteresis loop, which was calculated using a drafting software, and A_T is the area within a right triangle extending from the origin to the peak of the curve, defined as follows:

$$A_T = \frac{1}{2}\frac{\left(abs(\tau_{max}) + abs(\tau_{min})\right)}{2}\frac{\left(abs(\gamma_{max}) + abs(\gamma_{min})\right)}{2} \qquad (3)$$

Values of normalized shear modulus G/G_1 are plotted during cyclic loading for each stage (i.e., each γ_a) of test SS3 in Figure 9(a), where G is the shear modulus for each cycle and G_1 is the shear modulus for the first cycle of loading. The normalized shear modulus increases gradually throughout each stage as a result of continuing volumetric contraction (Fig. 4c). The normalized damping ratio D/D_1 is plotted similarly in Figure 9(b), where D is the damping ratio for each cycle and D_1 is the damping ratio for the first cycle of loading. For each stage, values slightly decrease and then approach a relatively stable value at high number of cycles. Similar trends were observed for the other tests.

Representative values of shear modulus and damping ratio were calculated for each test stage as an average over the last five cycles. In the few cases where slack in the system affected the hysteresis loops, the peaks of unaffected hysteresis loops were used to obtain the average shear modulus and damping ratio. Figure 10(a) presents the shear modulus reduction curve (i.e., G vs. log γ_a) for each test. Similar to natural soils, shear modulus decreases nonlinearly with increasing shear strain amplitude for each vertical stress. The testing program did not include, and the device may not be capable of producing, very low shear strain levels associated with the small strain shear modulus G_{max}. Figure 10(a) also shows that shear modulus increases with increasing vertical stress for each cyclic shear strain amplitude. Despite the difference in strain history, the data from test SS1 follows a consistent trend with the other three tests. The secant shear modulus of Type B TDA ranges from 200 to 3355 kPa, which is similar in order of magnitude to values reported in Table 1 for tire chips and granulated rubber with smaller particle sizes at similar cyclic shear strain amplitudes (Feng and Sutterer 2000; Kaneko et al. 2003; Hazarika et al. 2010).

A corresponding plot of damping ratio vs. cyclic shear strain amplitude is shown in Figure 10(b). At the smallest amplitude (0.1%), damping ratio ranges from 21% to 24% and is greater than typical values for natural granular soils at similar amplitudes, which might be expected to range from approximately 5 to 20% (e.g., Seed and Idriss 1970; Seed et al. 1986; Rollins et al. 1998). Damping ratio decreases and then increases with increasing γ_a for each test, and shows close agreement for all four vertical stress levels. The shape of the relationships in Figure 10(b) is similar to that reported for one of the tests on granulated rubber conducted by Feng and Sutterer (2000) at a confining stress of 345 kPa (the other tests in that study showed consistently increasing damping ratio). A comparison of the damping ratios from the previous studies listed in Table 1 indicates that the magnitudes reported by Feng and Sutterer (2000) were smaller (≤ 6%) but the strain ranges under investigation were much smaller. The damping ratios obtained from a reinterpretation of the data from Kaneko et al. (2003) and Hazarika et al. (2010) reported in Table 1 have similar magnitudes as those observed in the current study because their cyclic strain amplitudes were on the same order of magnitude as in this study. Interestingly, the decreasing/increasing trend in Fig. 10(b) is similar to the trend shown by Nye and Fox (2007) for cyclic shear tests on a hydrated needle-punched geosynthetic clay liner (GCL).

An evaluation of the repeatability of the shear modulus and damping ratio values obtained from the application of the same cyclic shear strain magnitudes to different specimens in test SS1 is shown in Figure 11. Despite the different specimens, which may have had slightly different structure and density, values of shear modulus and damping ratio are in close agreement at each strain amplitude.

Variation of shear modulus with vertical stress for all four tests is presented in Figure 13. Although values at the smallest cyclic shear strain amplitude of 0.1% do not correspond to small strains, these values follow a trend with vertical stress that is similar to the power law relationship of Hardin and Black (1966), which can be expressed as follows, neglecting the effects of void ratio and overconsolidation ratio:

$$\mathrm{G} = \mathrm{A}\left(\frac{\sigma_v}{P_{atm}}\right)^n \tag{4}$$

where σ_v is the vertical normal stress, P_{atm} is the atmospheric pressure (101.3 kPa), and A and n are fitting parameters. Best-fit curves and the corresponding equations, as obtained using Eq. (4) with nonlinear regression, are also show in Figure 13. Close agreement is observed for each shear strain amplitude for Type B TDA, with n values ranging from 0.48 to 0.71 and increasing with increasing strain amplitude. The value of *n* is typically assumed to be 0.5 for granular soils, and the parameters in Figure 12 indicate that this assumption may also be suitable for Type B TDA except for the two highest shear strain amplitudes where higher *n* values are needed..

Although sufficiently small cyclic shear strain amplitudes were not applied to measure G_{max} in the current study, the value of G_{max} may be inferred by fitting established shear modulus reduction curves to the data in Figure 10(a). The model of Darandeli (2001) was used and is described as follows:

$$\frac{G}{G_{max}} = \left(\frac{1}{1 + \left(\frac{\gamma}{\gamma_r}\right)^a} \right) \quad (5)$$

where a is a fitting parameter, γ_r is a threshold shear strain, and G_{max} is assumed to follow the same trend with vertical normal stress given by Equation (4). Darandeli (2001) proposed an empirical equation to estimate the value of γ_r for granular soils, but the calculated values were too small to fit the experimental data in Figure 10(a). Accordingly, the following power law equation was used to characterize the effects of vertical normal stress on γ_r:

$$\gamma_r = \gamma_0 \left(\frac{\sigma_v}{P_{atm}}\right)^m \quad (6)$$

The values of A in Equation (4), a in Equation (5), and γ_0 and m in Equation (6) were varied to obtain the best fit to the experimental data in Figure 10(a), and the resulting modulus reduction curves using A = 5100 kPa, a = 0.80, γ_0 = 0.6, and m = 0.55 are shown in Figure 13(a) and 13(b) in terms of the shear modulus and the normalized shear modulus G/G_{max}, respectively. Although some discrepancy is noted, the model provides a reasonable overall fit to the experimental data for Type B TDA. An alternative approach would be to measure the small-strain shear modulus in the laboratory or field using a wave propagation technique, and then modify the shear modulus trends reported in the current study to estimate project-specific modulus reduction curves.

For comparison, the results from Stokoe et al. (1994) can be used to estimate the shear modulus of compacted sand at a similar stress state as that evaluated for Type B TDA. Stokoe et al. (1994) observed that the shear modulus of remolded sand decreases about 40% from the value at small strain to the value at γ_a = 0.1%. The shear modulus of sand at a confining stress of 80 kPa and γ_a = 0.1% is approximately 32000 kPa, which is about 10 times larger than the highest value observed for Type B TDA in the current study. Stokoe et al. (1994) also reported that the damping ratio increased by about 10 times during application of cyclic shear strains from small strain up to 0.1%. Considering the minimum damping ratio for sands at a confining stress of 80 kPa is approximately 0.6%, the damping ratio at $\gamma_a = 0.1\%$ is expected to be approximately 6%. This is much smaller than the values calculated for Type B TDA. As such, TDA may not have as high of a shear modulus as compacted sands, but has much higher damping. Thus, Fills made of Type B TDA may experience greater displacements than granular soils during seismic events, and also may dissipate more energy depending on the frequency content of the motion and the fundamental mode of the structure.

CONCLUSIONS

Large-scale cyclic simple shear tests were conducted to measure and better understand the cyclic properties and behavior of Type B Tire Derived Aggregate (TDA) with large particle size. The cyclic simple shear tests were performed for vertical stresses ranging from 19.3 to 76.6 kPa and shear strain amplitudes ranging from 0.1% to 10%. The observed shear stress-shear strain hysteresis loops were similar to those of granular soils, with a lower shear modulus and a significantly larger damping ratio. The shear modulus of Type B TDA has a maximum value of 3,355 kPa and decreases with increasing shear strain amplitude, which is smaller in magnitude and similar in trend to natural granular soils in this vertical stress range. Similar to granular soils, the shear modulus increased nonlinearly with increasing vertical stress following a power law relationship. The damping ratio for Type B TDA showed a different behavior from granular soils, with a relatively high magnitude of 20 to 25% at the lowest shear strain amplitude (0.1%), followed by a decreasing/increasing trend with increasing amplitude. The damping ratio was essentially independent of the vertical stress level. Continuous contraction of the Type B TDA was observed during the cyclic shearing process for all vertical stress levels. The dynamic properties of Type B TDA presented in this paper are the most reliable values yet obtained and should be useful to avoid the over-conservatism often necessary with assumed parameters.

ACKNOWLEDGMENTS

Financial support from California Department of Resources Recycling and Recovery (CalRecycle) for project DRR11064, and in particular the assistance of Stacey Patenaude and Bob Fujii of CalRecycle and Joaquin Wright of GHD Consultants, Sacramento, is gratefully acknowledged. The authors also thank the staff of the Powell Laboratories at UCSD for assistance with the experimental work. The contents of this paper reflect the views of the authors and do not necessarily reflect the views of the sponsor.

APPENDIX I. REFERENCES

Ahn, I., Cheng, L., Fox, P.J., Wright, J., Patenaude, S., and Fujii, B. (2014). "Material properties of large-size tire derived aggregate for civil engineering applications." Journal of Materials in Civil Engineering, DOI: 10.1061/(ASCE)MT.1943-5533.0001225, 04014258.

Ahn, I.-S., and Cheng, L. (2014). "Tire derived aggregate for retaining wall backfill under earthquake loading." Construction and Building Materials. 57, 105-116.

American Society for Testing and Materials. (2012) ASTM D6270: Standard Practice for Use of Scrap Tires in Civil Engineering Applications. ASTM International, West Conshohocken, PA.

Anastasiadis, A., Senetakis, K., Pitilakis, K., Gargala, C., and Karakasi, I. (2012a). "Dynamic behavior of sand/rubber mixtures. Part 1: Effect of rubber content and duration of confinement on small-strain shear modulus and damping ratio." Journal of ASTM International. 9(2), 1-19.

Anastasiadis, A., Senetakis, K., Pitilakis, K. (2012). "Small strain shear modulus and damping ratio of sand/rubber and gravel/rubber mixtures." Journal of Geotechnical and Geological Engineering. 30(2), 363-382.

Eldin, (1993). "Construction and performance of shredded waste tire test embankment." Transportation Research Record. Transportation Research Board, Washington, DC. Volume 1345, 44-52.

Bosscher, P.J., Edil, T.B., and Kuraoka, S. (1997). "Design of highway embankments using tire chips." Journal of Geotechnical and Geoenvironmental Engineering. 123(4), 295-304.

CalRecycle. (2016a). California Waste Tire Market Report: 2015. Publication # DRRR 2016-01567. Sacramento, CA.

CalRecycle. (2016b). Usage Guide: Tire-Derived Aggregate (TDA). Publication # DRRR 2016-01545. Sacramento, CA.

CalRecycle. (2011). Civil Engineering Applications Using Tire Derived Aggregate (TDA). Publication # DRRR-2011-038. Sacramento, CA.

Darendeli, M.B. (2001). Development of a New Family of Normalized Modulus Reduction and Material Damping Curves. PhD Dissertation, Univ. of Texas. Austin, Tex.

Dickson, T.H., Dwyer, D.F., Humphrey, D.N. (2001). "Prototype tire-shred embankment construction." Transportation Research Record, 1755, National Research Council, Transportation Research Board, Washington, D.C. pp. 160-167.

Edil, T.B. and Bosscher, P.J. (1994). "Engineering properties of tire chips and soil mixtures." Geotechnical Testing Journal, 17(4), 453-464.

Ehsani, M., Shariatmadari, N., Mirhosseini, S.M. (2015). "Shear modulus and damping ratio of sand-granulated rubber mixtures." J. Cent. South Univ. 22, 3159−3167.

Feng, Z.Y. and Sutterer, K.G. (2000). “Dynamic properties of granulated rubber/sand mixtures.” ASTM Geotechnical Testing Journal. 23(3), 338–344.

Fox, P.J., Sanders, M., Latham, C., Ghaaowd, I., and McCartney, J.S. (2017). “Large-scale direct-simple shear test for large-particle tire-derived aggregates.” ASTM Geotechnical Testing Journal. Accepted.

Geosyntec. (2008). Guidance Manual for Engineering Uses of Scrap Tires. Prepared for Maryland Department of the Environment. Geosyntec Project No.: ME0012-11.

Ghaaowd, I., McCartney, J.S., Thielmann, S.S., Sanders, M.J., and Fox, P.J. (2017). “Shearing behavior of tire derived aggregate with large particle size. I. Internal and concrete interface direct shear.” Journal of Geotechnical and Geoenvironmental Engineering. Companion paper.

Hardin, B.O. and Black, W.L. (1966). “Sand stiffness under various triaxial stresses. ASCE Journal of the Soil Mechanics and Foundation Division. 92(SM2), 27-42.

Hazarika, H., Yasuhara, K., Kamokar, A.K., and Mitarai, Y. (2008). “Shaking table test on liquefaction prevention using tire chips and sand mixture.” In: Hazarika H, Yasuhara K, editors. International Workshop on Scrap Tire Derived Geomaterials: Opportunities and Challenges. Taylor and Francis. 215–22.

Hazarika, H., Kohama, E., and Sugano, T. (2008). “Underwater shake table tests on waterfront structures protected with tire chips cushion.” Journal of Geotechnical and Geoenvironmental Engineering. 134(12), 1706–1719.

Hazarika, H., Hyodo, M., and Yasuhara, K. (2010). “Investigation of tire chips-sand mixtures as preventative measure against liquefaction.” GeoShanghai 2010. ASCE. 338-345.

Hoppe, E.J. (1998). “Field study of shredded-tire embankment,” Transportation Research Record No. 1619, Transportation Research Board, Washington, DC. 47-54.

Hsu, C., Vucetic, M. (2004). “Volumetric threshold shear strain for cyclic settlement.” Journal of Geotechnical and Geoenvironmental Engineering. 130(1), 58-70

Humphrey, D., Sandford, T., Cribbs, M., and Manion, W. (1993). “Shear strength and compressibility of tire chips for use as retaining wall backfill.” Transportation Research Record. Transportation Research Board, Washington, DC. Volume 1422, 29–35.

Kaneko, T., Orense, R.P., Hyodo, M., and Yoshimoto, N. (2003). “Seismic response characteristics of saturated sand deposits mixed with tire chips.” Journal of Geotechnical and Geoenvironmental Engineering. 139(4), 633-643.

Lee, K.L., and Albaisa, A. (1974). “Earthquake induced settlements in saturated sands.” Journal of the Geotechnical Engineering Division. ASCE, 103(6), 535-547.

Lee, H.J. and Roh, H.S. (2007). “The use of recycled tire chips to minimize dynamic earth pressure during compaction of backfill.” Construction and Building Materials. 21, 1016–1026.

Lee, K.L., and Seed, H.B. (1967). “Drained strength characteristics of sands.” Journal of the Soil Mechanics and Foundation Division. SM6, 118-143.

Mashiri, M.S., Sheikh, M., Neaz., V.J. and Tsang, H. (2013). “Dynamic properties of sand-tyre chip mixtures.” Australian Earthquake Engineering Society Conference. S. Anderson, Ed. Australian Earthquake Engineering Society, Tasmania. 1-8.

Nakhaei, A. Marandi, S.M., Sani Kermani, S., Bagheripour, M.H. (2012). “Dynamic properties of granular soil mixed with granulated rubber.” Soil Dynamics and Earthquake Engineering. 43, 124-232.

Nye, C.J., and Fox, P.J. (2007). "Dynamic shear behavior of a needle-punched geosynthetic clay liner." Journal of Geotechnical and Geoenvironmental Engineering. 133(8), 973-983.

Rollins, K.M., Evans, M., Diehl, N., and Daily, W. (1998). "Shear modulus and damping relationships for gravels." Journal of Geotechnical and Geoenvironmental Engineering. 124(5), 396-405.

Seed, H.B., and Idriss, I.M. (1970). "Soil moduli and damping factors for dynamic response analysis." Rep. No. EERC 70-10, Earthquake Engineering Research Center, Berkeley, Calif.

Seed, H.B., Wong, R.T., Idriss, I.M., and Tokimatsu, K. (1986). "Moduli and damping factors for dynamic analyses of cohesionless soils." Journal of Geotechnical Engineering. 112(11), 1016-1032.

Senetakis, K., Anastasiadis, A., Pitilakis, K., Souli, A. (2012a). "Dynamic behavior of sand/rubber mixtures, Part II: Effect of rubber content on G/GO-c-DT curves and volumetric threshold strain. Journal of ASTM International, 9(12), 1-12.

Senetakis, K., Anastasiadis, A., Pitilakis, K. (2012b). "Dynamic properties of dry sand/rubber (SRM) and gravel/rubber (GRM) mixtures in a wide range of shearing strain amplitudes." Soil Dynamics and Earthquake Engineering. 33, 38-53.

Silver, M.L., and Seed, H.B. (1971). "Volume changes in sands during cyclic loading." Journal of Soil Mechanics and Foundations Division. 97(SM9), 1171-1182.

Stokoe, K.H., III, Hwang, S. K., and Lee, J. N.-K., and Andrus, R. (1995). "Effects of various parameters on the stiffness and damping of soils at small to medium strains." Proceedings of 1st International Symp. On Pre-failure Deformation Characteristics of Geomaterials. Vol. 2, 785-816.

Tandon, V., Velazco, D.A., Nazarian, S., and Picornell, M. (2007). “Performance monitoring of embankments containing tire chips: Case study.” Journal of Performance of Constructed Facilities. 21(3), 207–214.

Whang, D., Riemer, M.F., Bray, J.D., Stewart, J.P., and Smith, P.M. (2000). “Characterization of seismic-compression of some compacted fills.” Geo-Denver Conference, ASCE, Denver, CO., 180-194.

Tsang, H.H. (2008). “Seismic isolation by rubber–soil mixtures for developing countries.” Earthquake Engineering and Structural Dynamics. 37(2), 283–303.

Xiao, M., Ledezma, M., and Hartman, C. (2013). “Shear resistance of tire-derived aggregate using large-scale direct shear tests. Journal of Materials in Civil Engineering. 04014110-1-8.

Xiao, M., Bowen, J., Graham, M., and Larralde, J. (2012). “Comparison of seismic responses of geosynthetically-reinforced walls with tire-derived aggregates and granular backfills.” Journal of Materials in Civil Engineering. 24(11), 1368-1377.

Youd, T. L. (1972). “Compaction of sands by repeated shear straining.” Journal of Soil Mechanics and Foundations Division, ASCE. 98(7), 709-725.

Table 1: Summary of previous studies involving the cyclic response of TDA (Note: damping ratio and shear modulus values from Kaneko et al. (2003) and Hazarika et al. (2010) reinterpreted from reported hysteresis loops)

Test Parameters and Results	**Feng and Sutterer (2000)**	**Kaneko et al. (2003)**	**Hazarika et al. (2010)**
Equipment type	Resonant column/ Torsional Shear	Cyclic simple shear	Cyclic triaxial
TDA type	Granulated rubber	Tire chips	Tire chips
TDA specific gravity	1.11	1.15	1.15
Specimen shape	Cylinder	Cylinder	Cylinder
Specimen diameter (mm)	70	60	50
Specimen height (mm)	150	40	100
Maximum TDA particle size (mm)	4.76	1.1	1.0
Saturation conditions	Dry	Saturated	Saturated
Confining stress range (kPa)	69-483	37.57-43.68	100
Cyclic strain range (%)	0.003-0.1	2.7-4.4	2.5
Damping ratio (%)	4.2-6.0	15.0-24.0	10.0
Shear modulus (kPa)	1100-2800	160-200	1484

Table 2: Summary of Type B TDA simple shear testing program

Test	**Shear Strain Amplitude (%)**	**Vertical Stress at Specimen Mid-Height, σ_v (kPa)**	**Initial Total Unit Weight (kN/m^3)**	**Initial Void Ratio**
SS1	0.1, 0.3, 1, 3, 0.3, 1, 3, 10	19.3	5.64	1.00
SS2	0.1, 0.3, 1, 3, 10	38.3	6.59	0.71
SS3	0.1, 0.3, 1, 3, 10	57.5	6.82	0.65
SS4	0.1, 0.3, 1, 3, 10	76.6	7.07	0.60

LIST OF FIGURE CAPTIONS

FIG. 1: Large scale combination direct shear/simple shear device in simple shear mode: (a) Schematic diagram; (b) Photograph

FIG. 2: Time histories for cyclic simple shear test SS1: (a) Horizontal displacement; (b) Shear force; (c) Volumetric strain

FIG. 3: Time histories for cyclic simple shear test SS2: (a) Horizontal displacement; (b) Shear force; (c) Volumetric strain

FIG. 4: Time histories for cyclic simple shear test SS3: (a) Horizontal displacement; (b) Shear force; (c) Volumetric strain

FIG. 5: Time histories for cyclic simple shear test SS4: (a) Horizontal displacement; (b) Shear force; (c) Volumetric strain

FIG. 6: Volumetric strain at the end of 20 cycles for each test stage

FIG. 7: Hysteresis loops for all cyclic shear strain amplitudes: (a) SS1, (b) SS2, (c) SS3; (d) SS4

FIG. 8: Backbone curves corresponding to 20 cycles of loading at four vertical stress levels

FIG. 9: Normalized shear modulus and normalized damping ratio for test SS3

FIG. 10: Effect of cyclic shear strain amplitude on average values of: (a) Shear modulus; (b) Damping ratio

FIG. 11: First specimen and second specimen properties for test SS1: (a) Shear modulus; (b) Damping ratio

FIG. 12: Effect of vertical stress and cyclic shear strain amplitude on shear modulus of Type B TDA

FIG. 13: Estimated shear modulus reduction curves for Type B TDA: (a) G vs. γ, (b) G/G_{max} vs. γ

Figure 1 Click here to download Figure Figure 01.tif

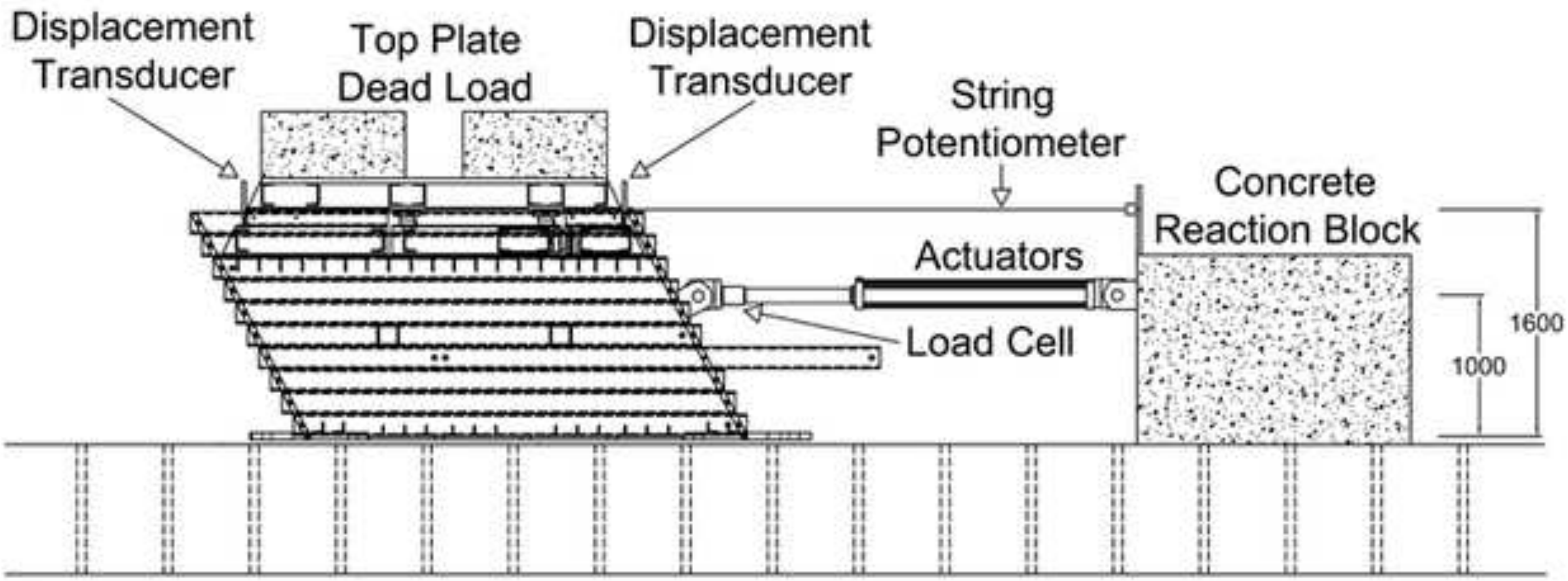

(a)

(b)

Figure 2

Click here to download Figure Figure 02.tif

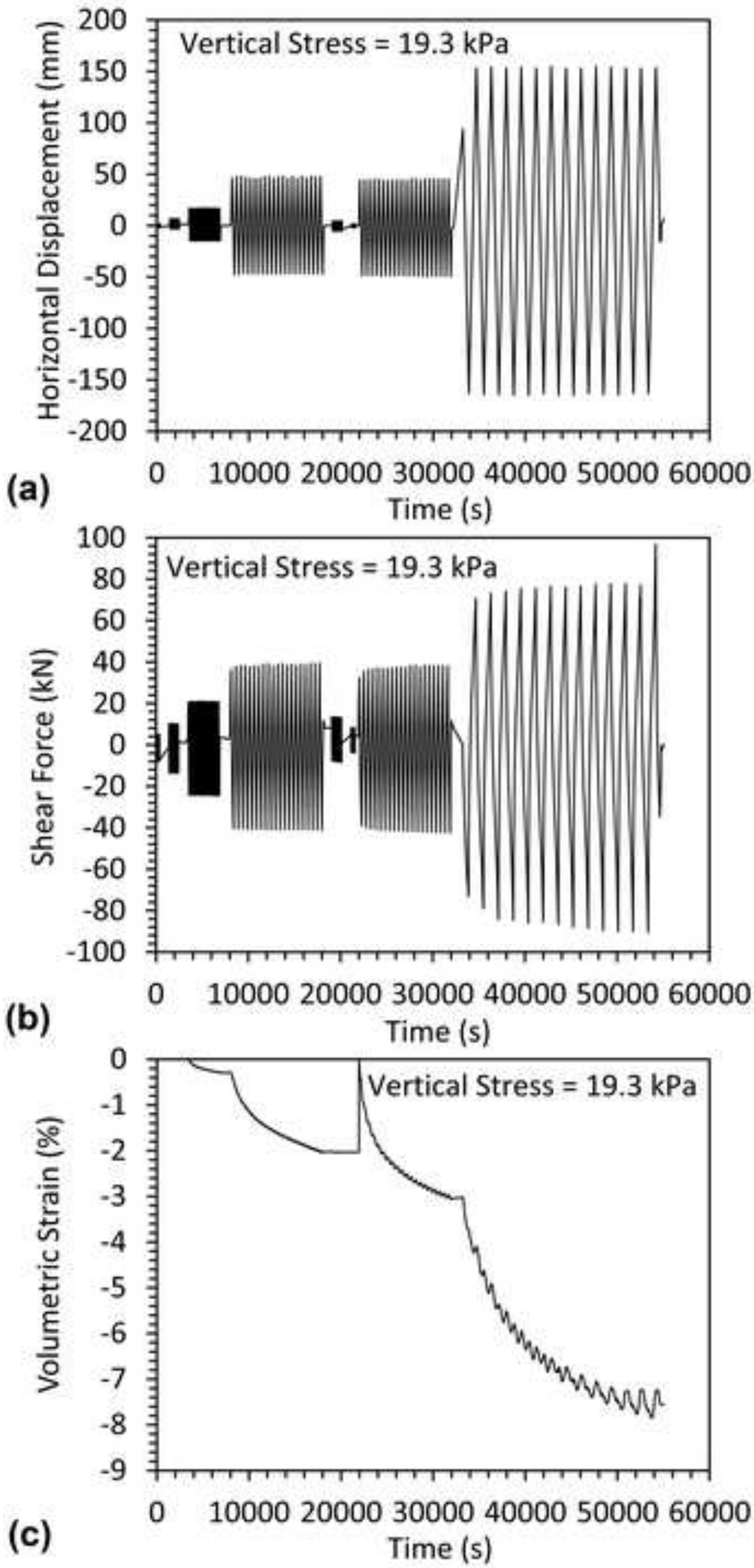

Figure 3

Click here to download Figure Figure 03.tif

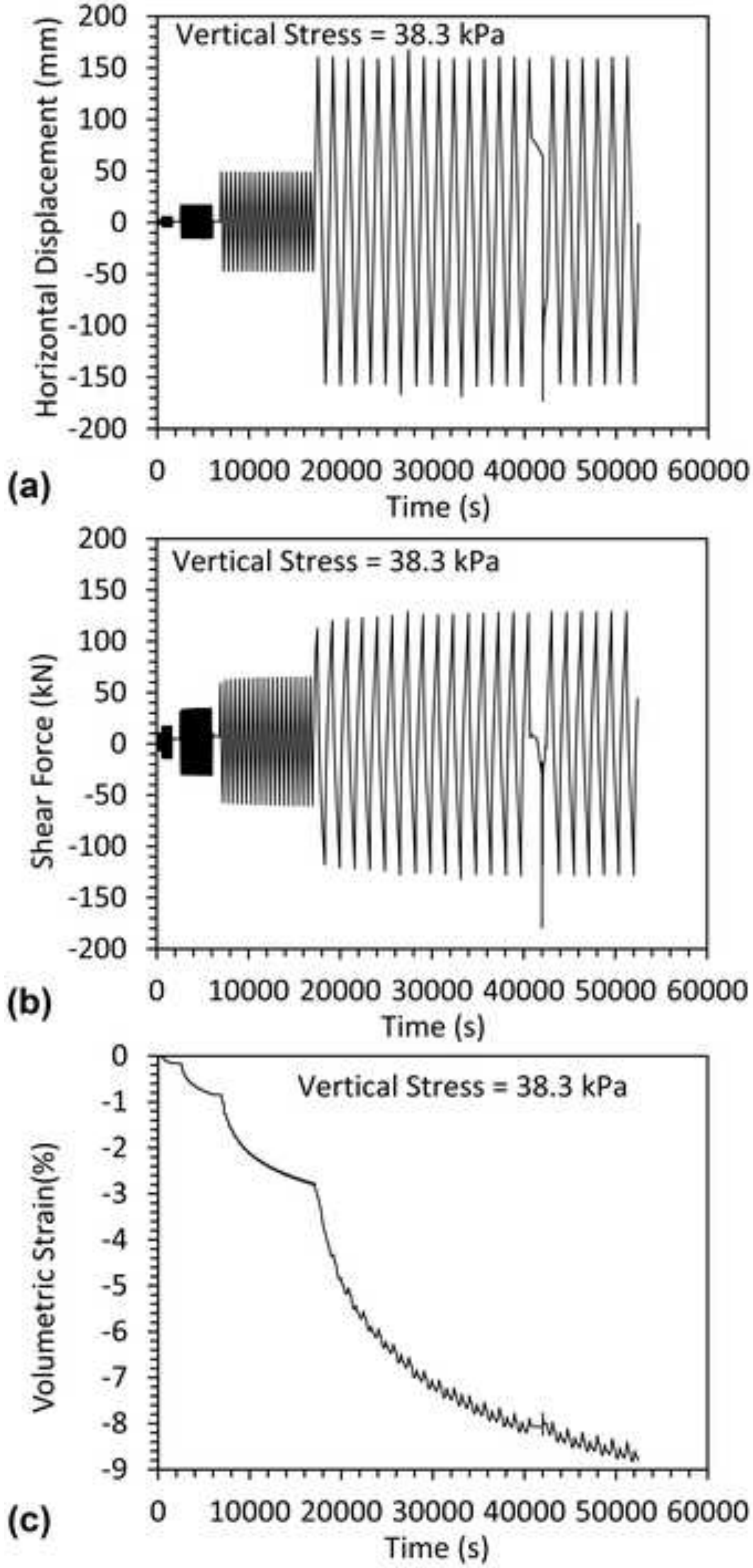

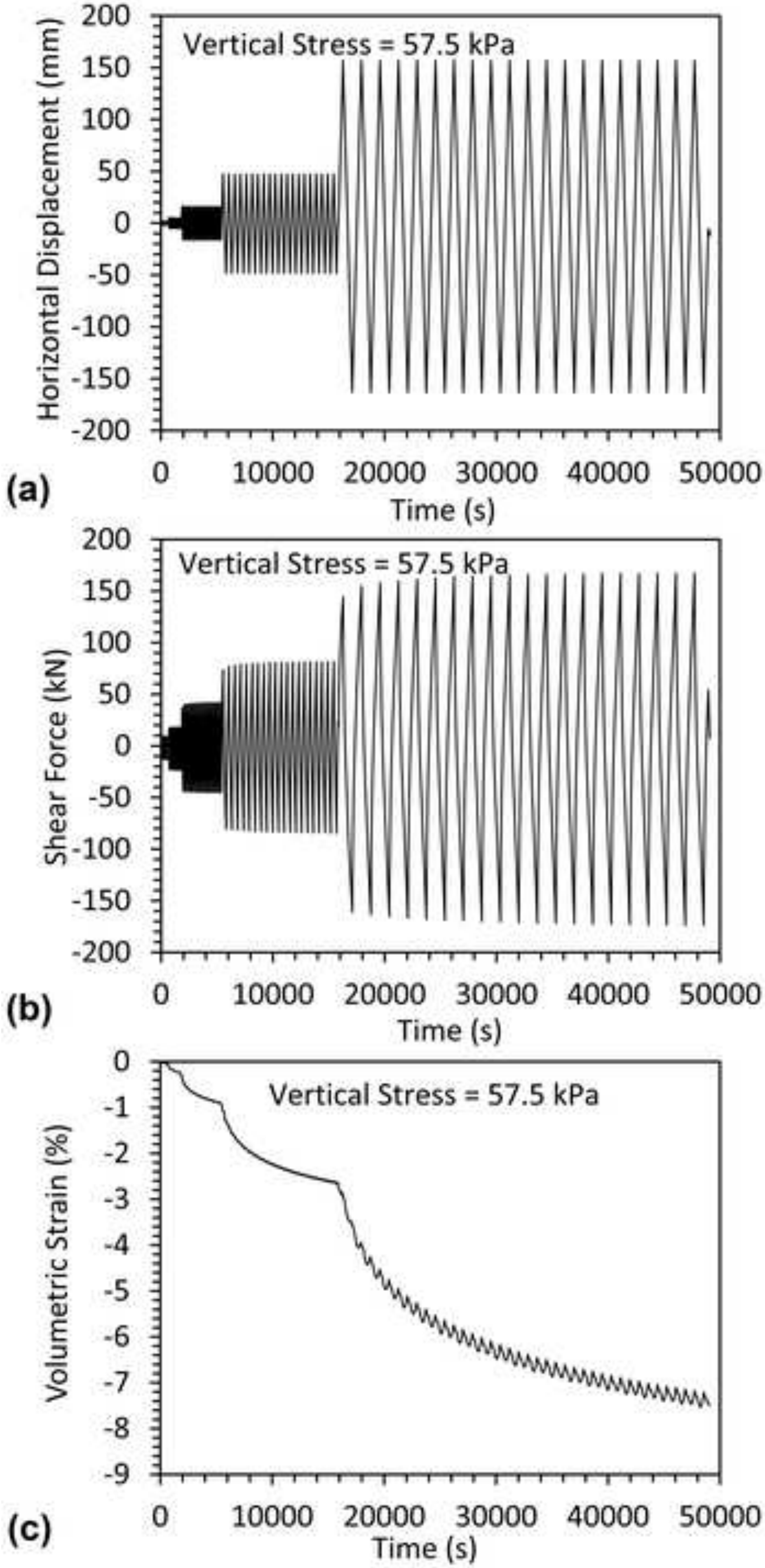
Vertical Stress = 57.5 kPa
Horizontal Displacement (mm)
200
150
100
50
0
-50
-100
-150
-200
(a)
0
10000
20000
30000
40000
50000
Time (s)
Vertical Stress = 57.5 kPa
Shear Force (kN)
(b)
Time (s)
Vertical Stress = 57.5 kPa
Volumetric Strain (%)
0
-1
-2
-3
-4
-5
-6
-7
-8
-9
(c)
Time (s)

Figure 5

Click here to download Figure Figure 05.tif

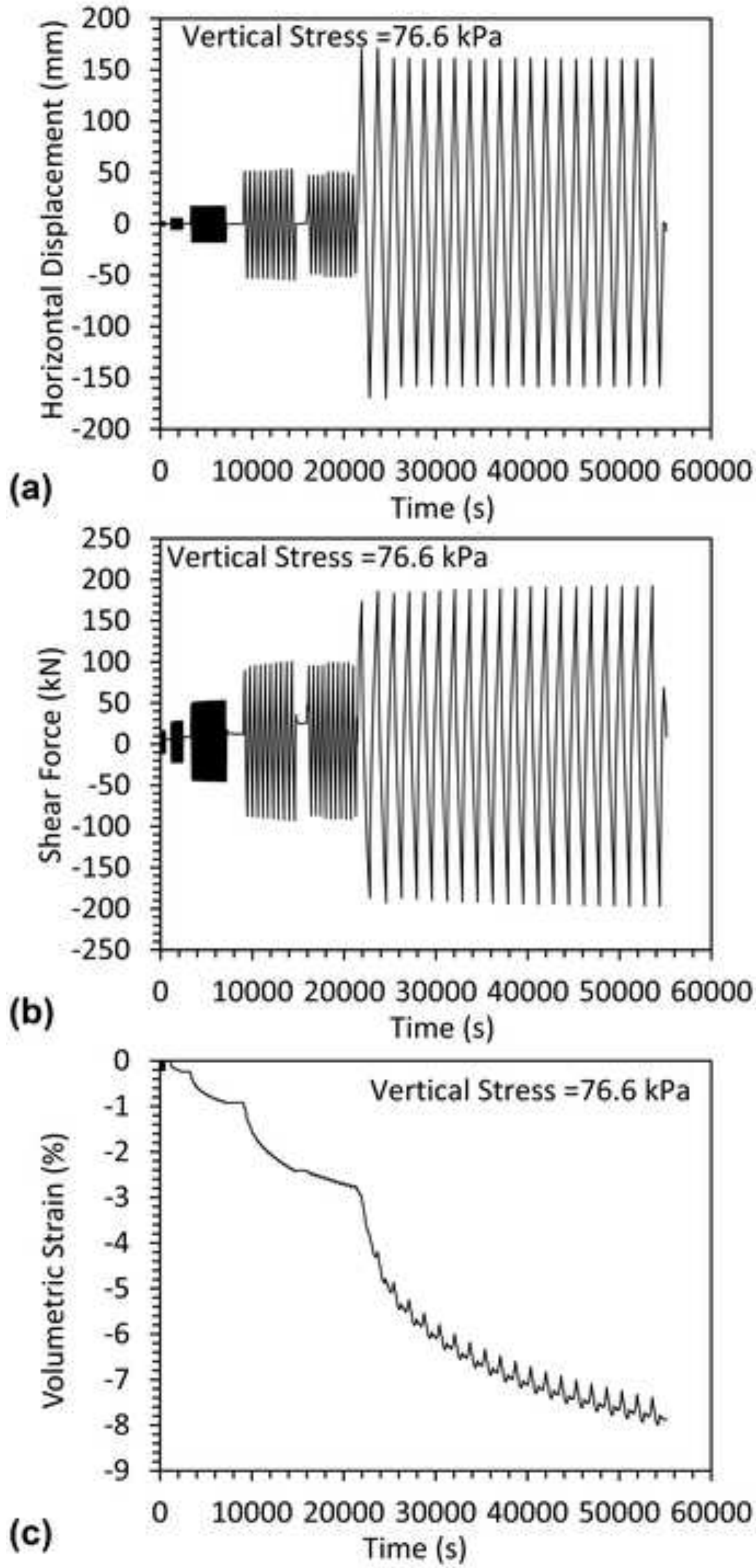

Figure 6

Click here to download Figure Figure 06.tif

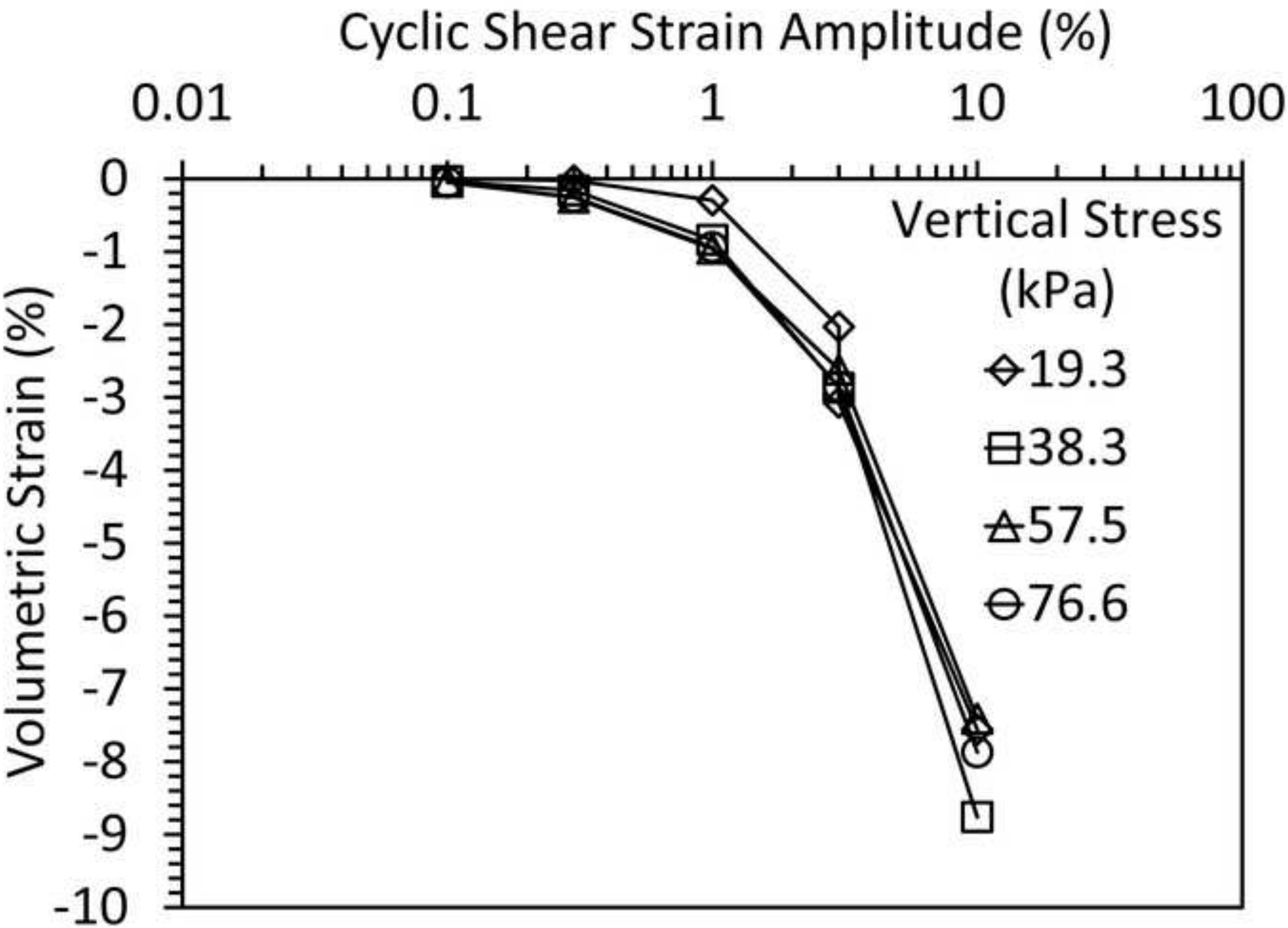

Figure 7

Click here to download Figure Figure 07.tif

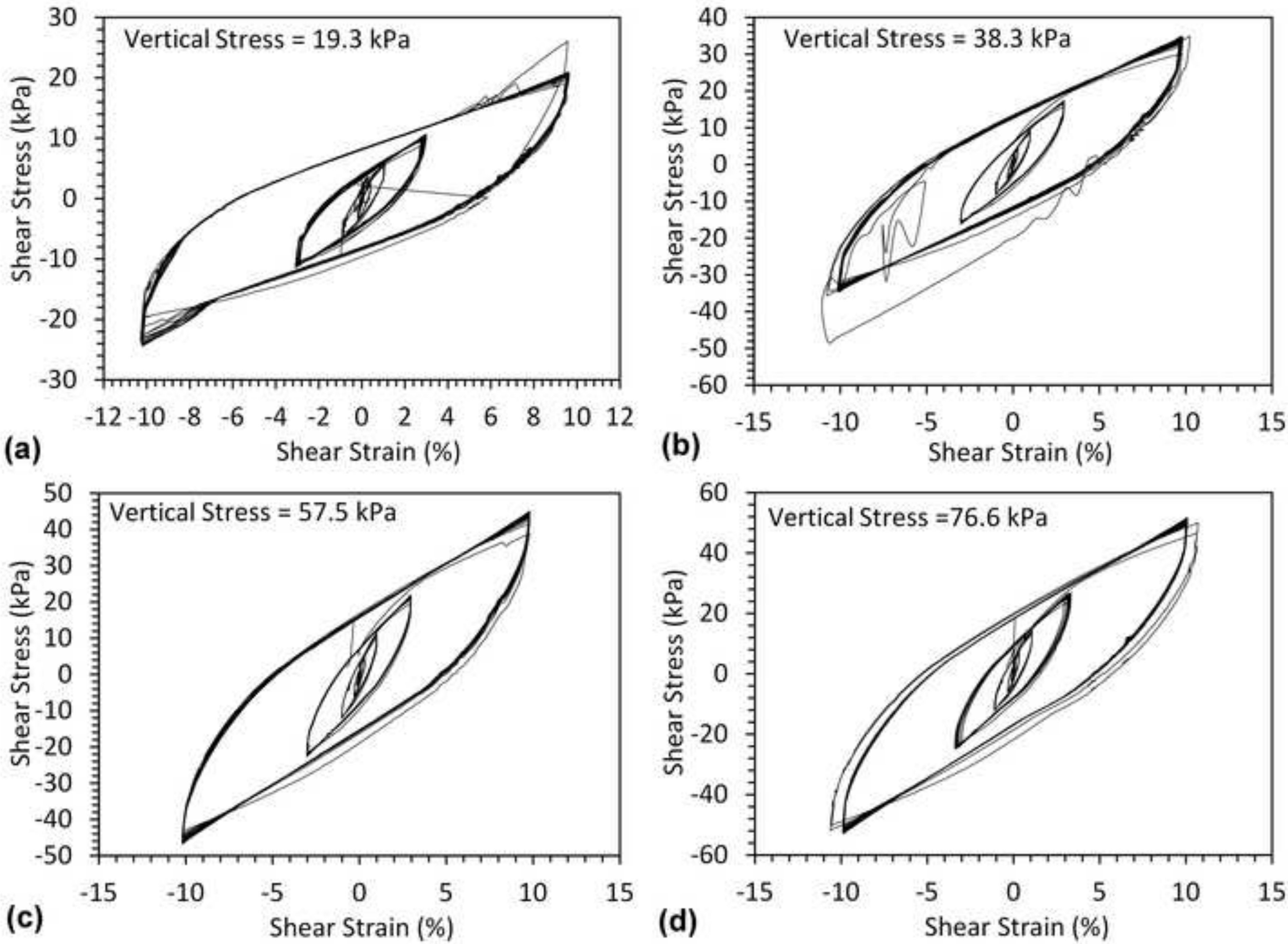

Figure 8

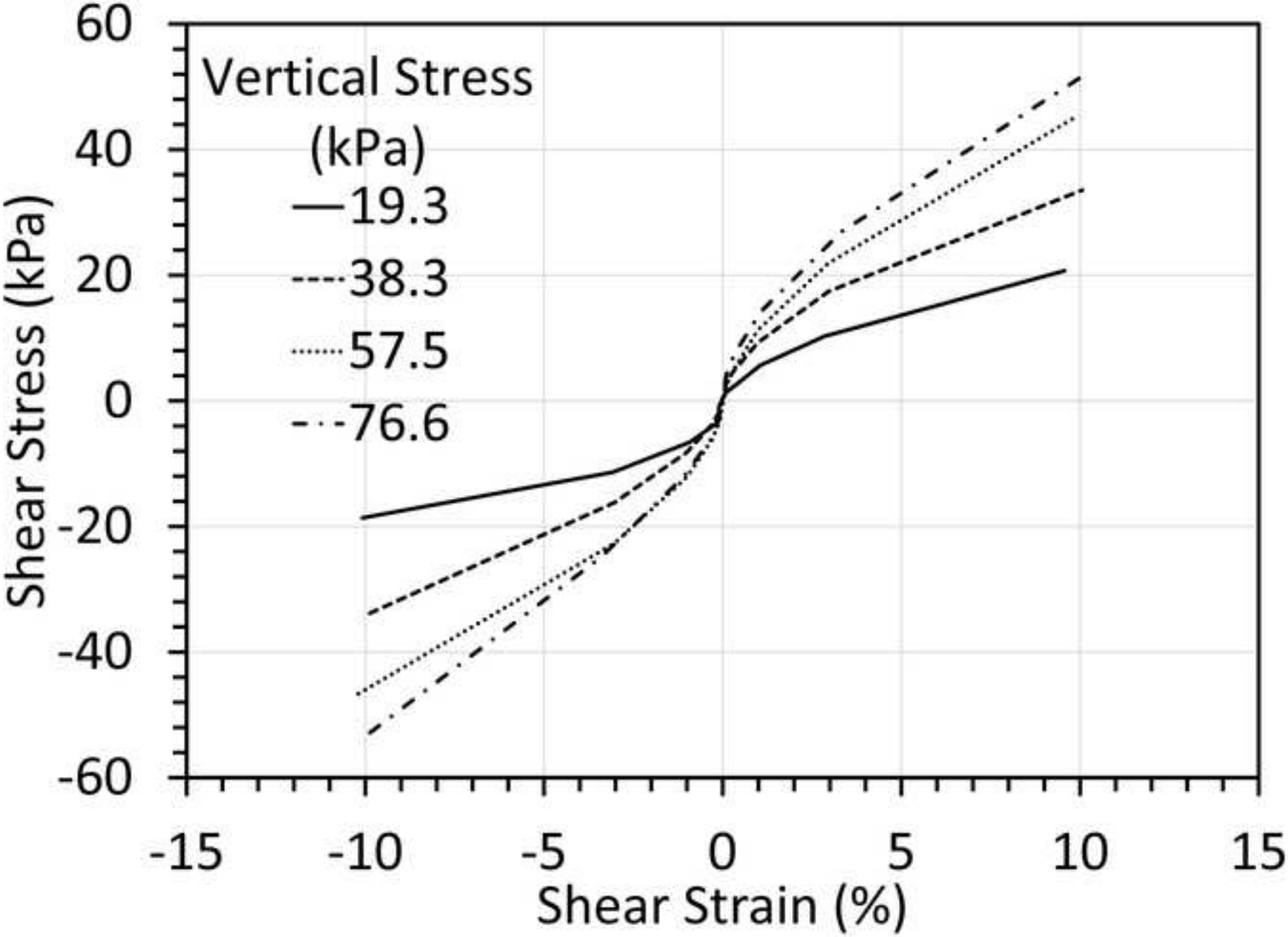
Vertical Stress (kPa)
19.3
38.3
57.5
76.6
Shear Stress (kPa)
60
40
20
0
-20
-40
-60
Shear Strain (%)
-15
-10
-5
0
5
10
15

Figure 9

Click here to download Figure Figure 09.tif

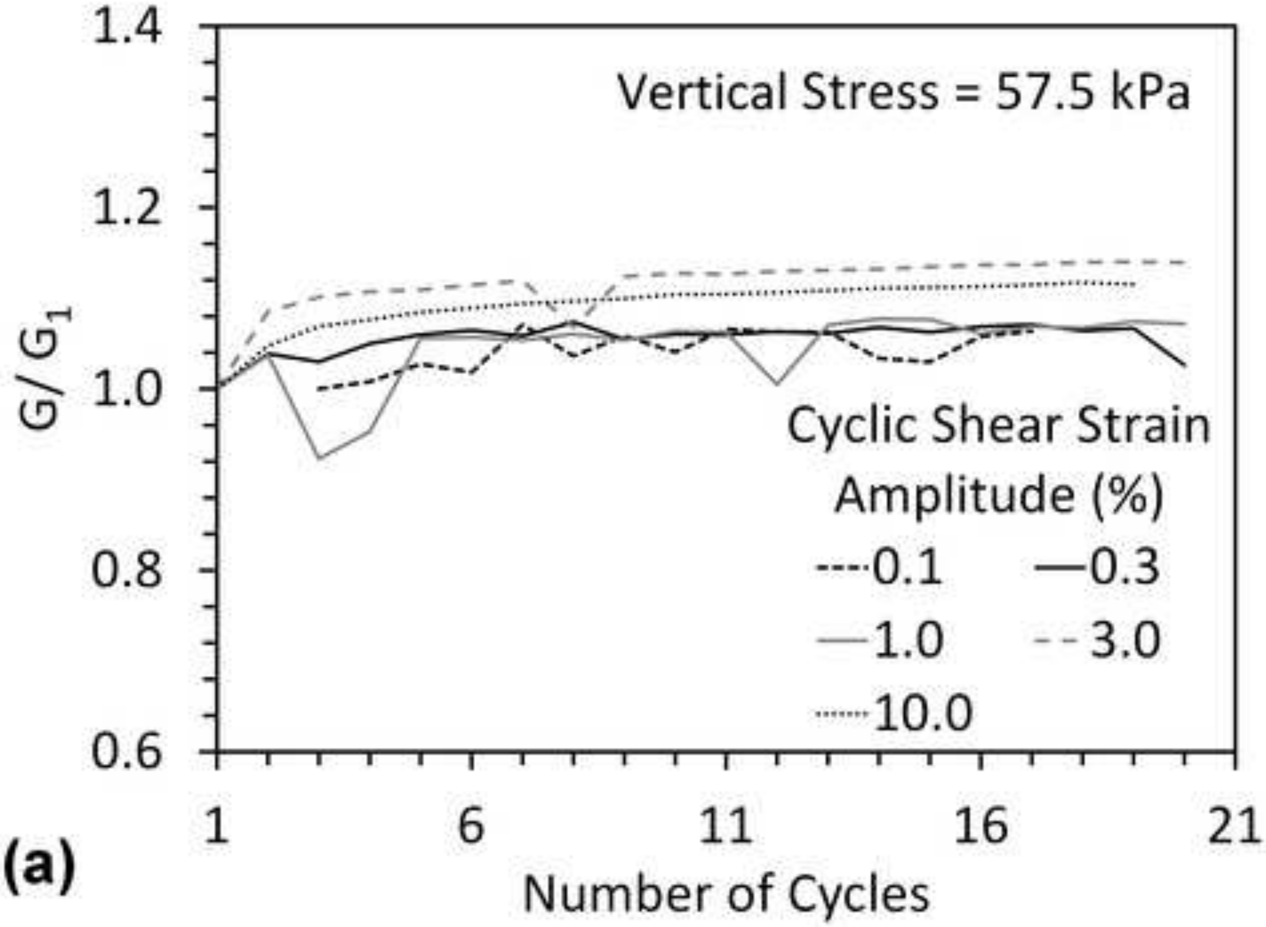

(a)

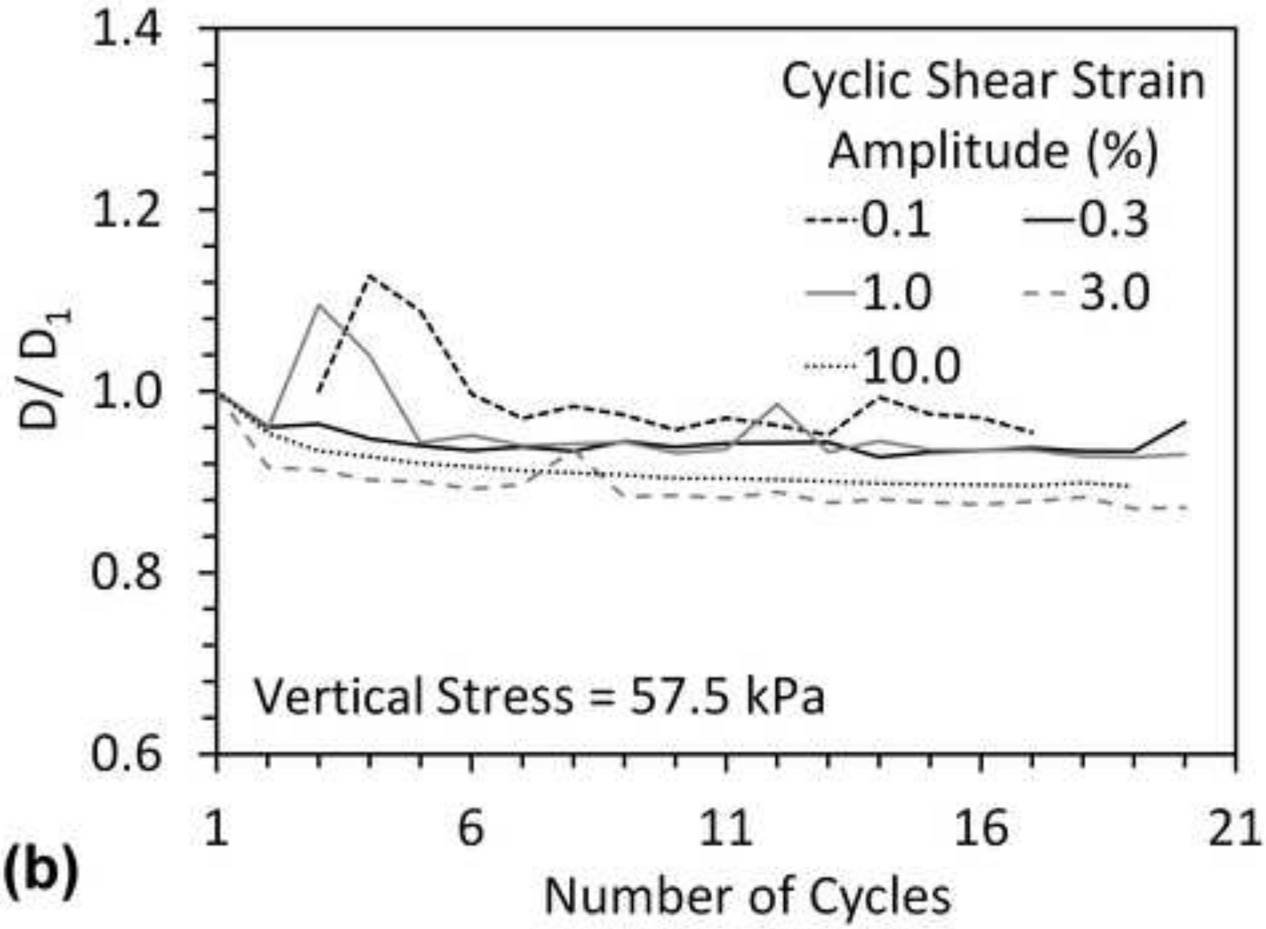

(b)

Figure 10

Click here to download Figure Figure 10.tif

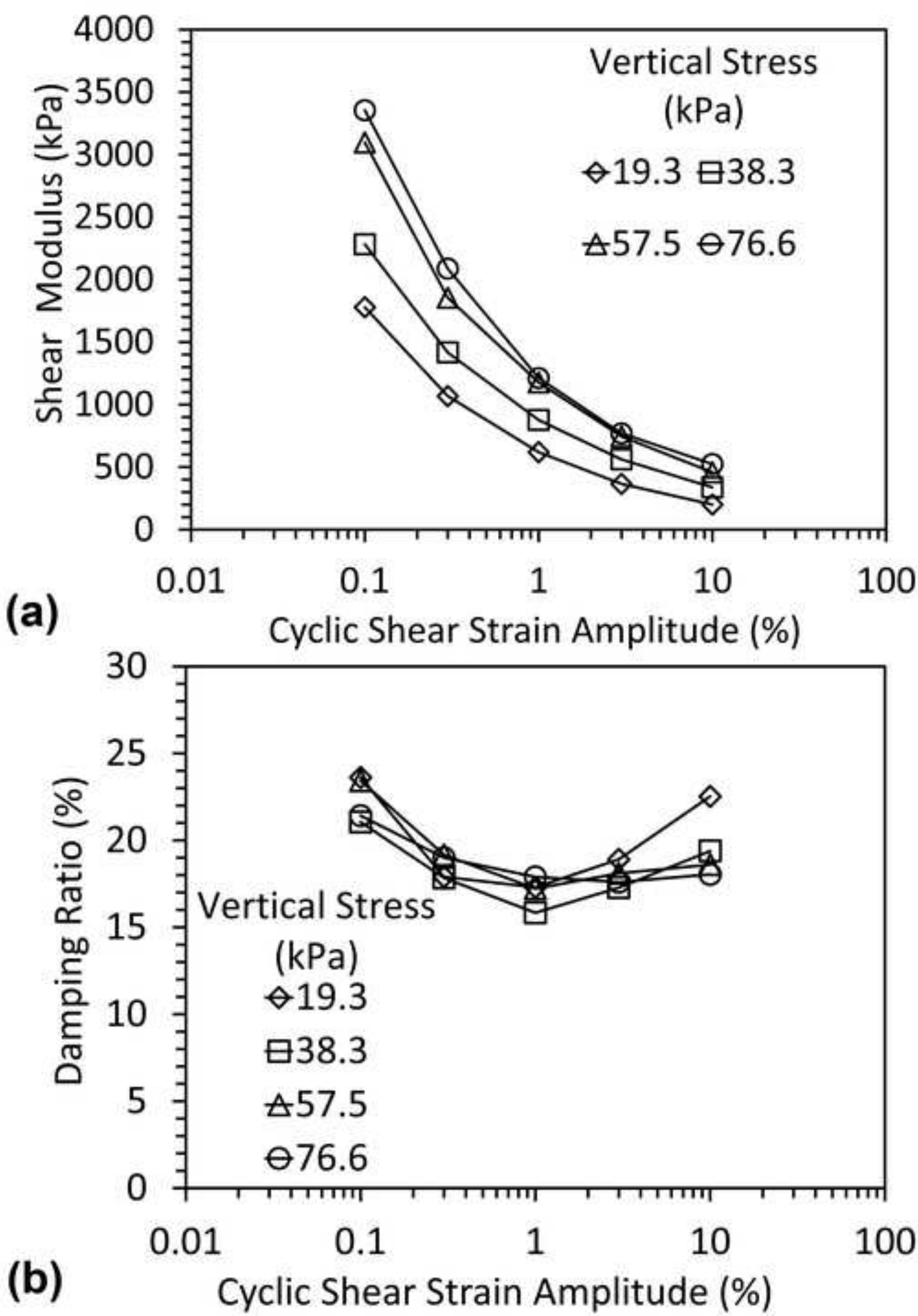

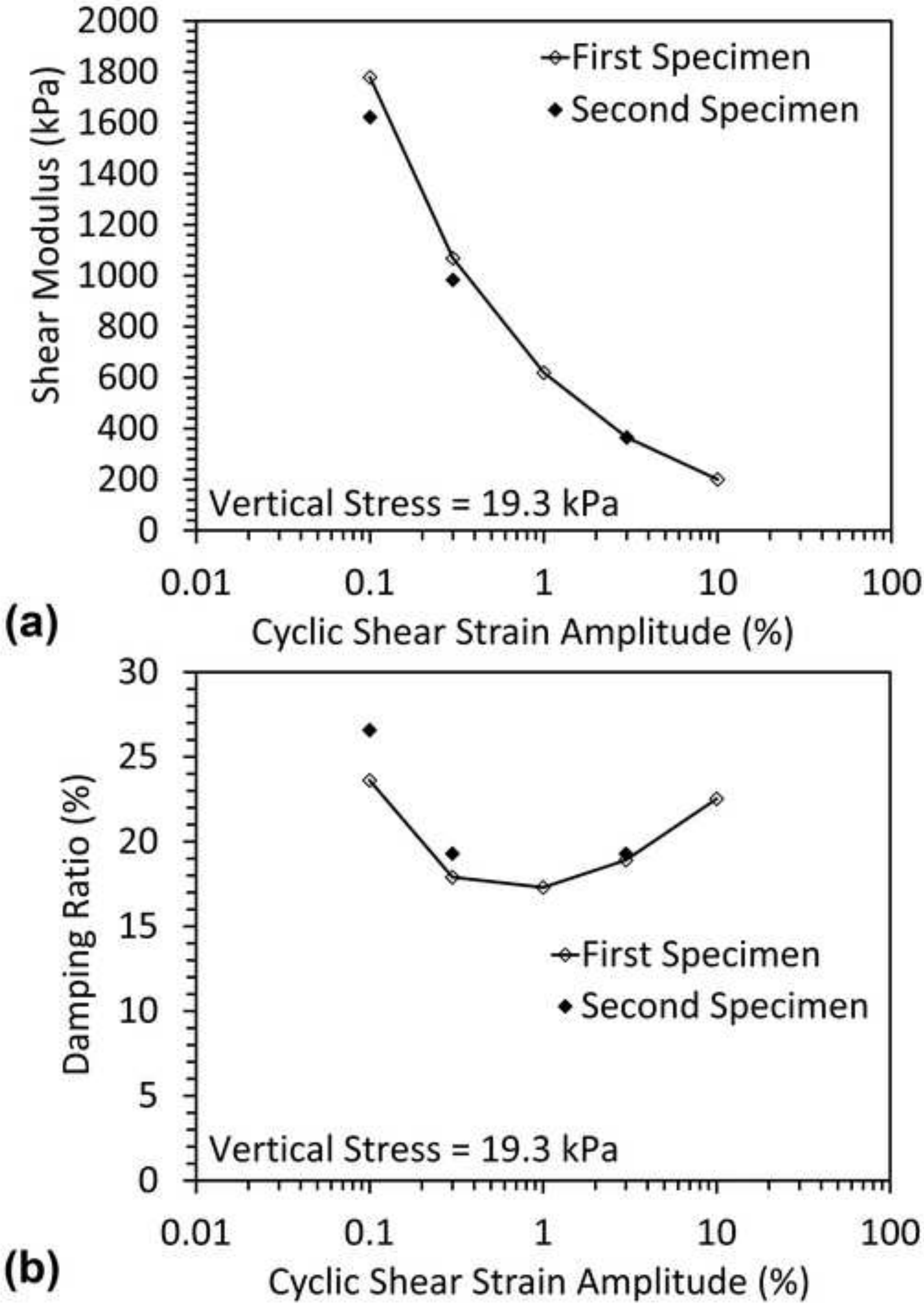
Shear Modulus (kPa)
2000
1800
1600
1400
1200
1000
800
600
400
200
0
First Specimen
Second Specimen
Vertical Stress = 19.3 kPa
0.01
0.1
1
10
100
(a)
Cyclic Shear Strain Amplitude (%)
Damping Ratio (%)
30
25
20
15
10
5
0
First Specimen
Second Specimen
Vertical Stress = 19.3 kPa
0.01
0.1
1
10
100
(b)
Cyclic Shear Strain Amplitude (%)

Figure 12

Click here to download Figure Figure 12.tif

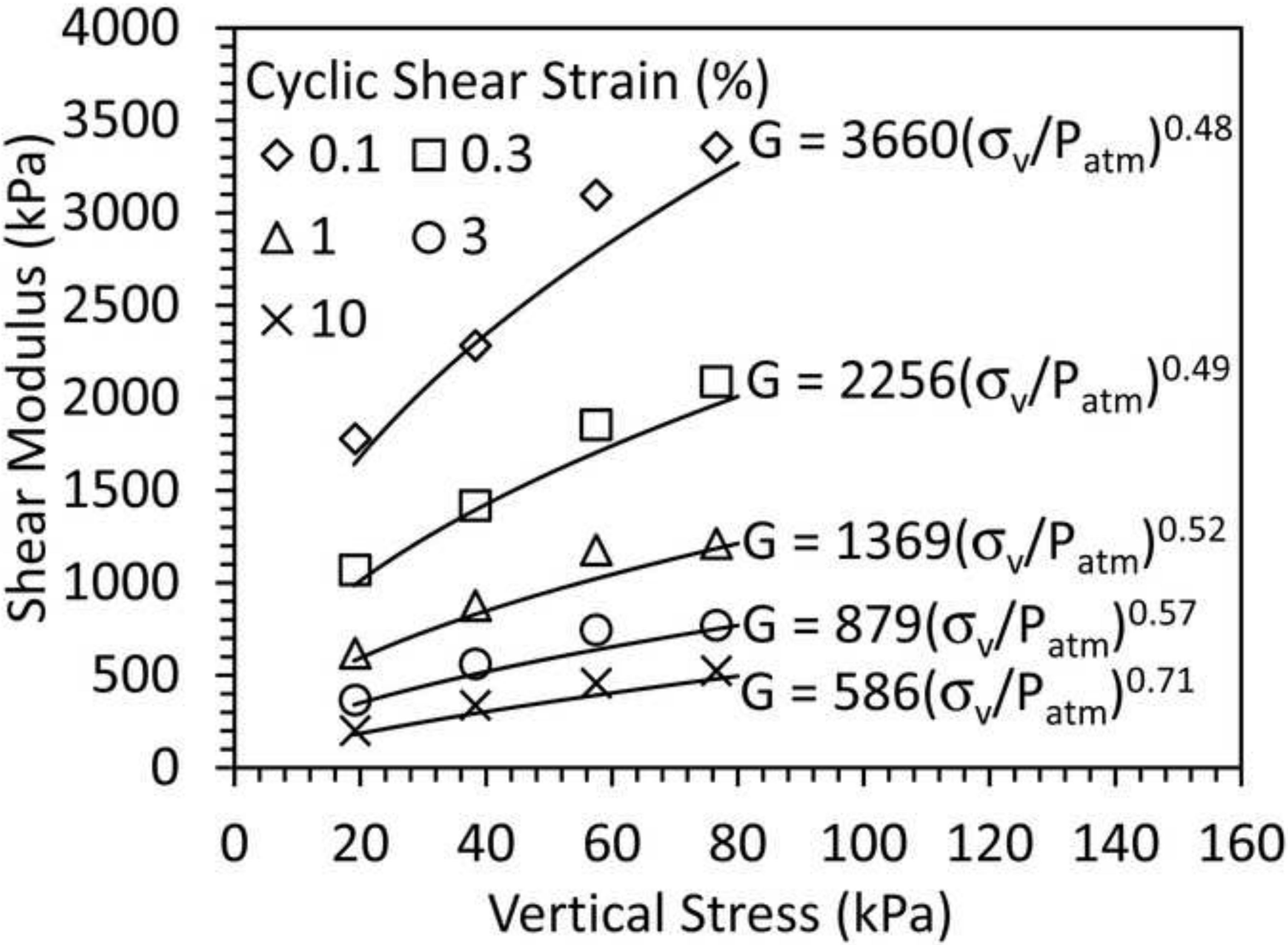

Figure 13

Click here to download Figure Figure 13.tif